Calculation of Forces at Focal Adhesions from Elastic Substrate Data: The Effect of Localized Force and the Need for Regularization

U. S. Schwarz,*[†] N. Q. Balaban,[‡§] D. Riveline,[§¶] A. Bershadsky,[§] B. Geiger,[§] and S. A. Safran[†]

*Max Planck Institute of Colloids and Interfaces, 14424 Potsdam, Germany; [†]Department of Materials and Interfaces, The Weizmann Institute of Science, Rehovot 76100, Israel; [‡]Laboratory of Living Matter, Rockefeller University, New York, New York 10021 USA; [§]Department of Molecular Cell Biology, The Weizmann Institute of Science, Rehovot 76100, Israel; and [¶]Laboratoire de Spectrométrie Physique, UMR 5588, Université Joseph Fourier-CNRS, BP 87, 38402 Saint Martin d'Hères Cedex, France

ABSTRACT   Forces exerted by stationary cells have been investigated on the level of single focal adhesions by combining elastic substrates, fluorescence labeling of focal adhesions, and the assumption of localized force when solving the inverse problem of linear elasticity theory. Data simulation confirms that the inverse problem is ill-posed in the presence of noise and shows that in general a regularization scheme is needed to arrive at a reliable force estimate. Spatial and force resolution are restricted by the smoothing action of the elastic kernel, depend on the details of the force and displacement patterns, and are estimated by data simulation. Corrections arising from the spatial distribution of force and from finite substrate size are treated in the framework of a force multipolar expansion. Our method is computationally cheap and could be used to study mechanical activity of cells in real time.

INTRODUCTION

In recent years, evidence has been growing for an important role of mechanical force in regulating the behavior of single cells and their communities (Chicurel et al., 1998; Galbraith and Sheetz, 1998; Geiger et al., 2001). Force on cells can be either external (e.g., resulting from blood flow or traction of other cells) or internal. For animal cells, internal force is mostly generated by the actin cytoskeleton and transmitted to the extracellular matrix (ECM) through cell-matrix adhesions. For stationary animal cells cultured on flat substrates, the most prominent type of cell-matrix adhesion are focal adhesions (FAs) (Burridge and Chrzanowska-Wodnicka, 1996; Geiger and Bershadsky, 2001). FAs are large supramolecular assemblies, consisting of a submembrane plaque with more than 50 different proteins (including vinculin and paxillin) and a transmembrane part provided by receptors of the integrin family. They can be detected as dark areas in interference reflection microscopy (Abercrombie and Dunn, 1975) and as regions of close approach in transmission electron microscopy (Chen and Singer, 1982). FAs are only one variant of the different types of cell-matrix adhesions, which develop in different situations; in particular, FAs have different morphologies and composition than cell-matrix adhesions in a physiological context (Cukierman et al., 2002). Nevertheless, they are excellent model systems for studying integrin-mediated crosstalk between extracellular matrix and cytoskeleton, which is not only ubiquitous under physiological conditions, but also relevant in the biotechnological context, e.g., when culturing cells on biochips. Forces exerted at FAs allow the cell to probe the mechanical properties of its environment (Pelham and Wang, 1997; Lo et al., 2000; Zamir et al., 2000). Successful adhesion of stationary cells implies forces being sustained at FAs, and several studies indicate that FAs function as mechanosensors, which feed directly into cellular regulation (Choquet et al., 1997; Riveline et al., 2001). In particularly, it has been shown that there is a close relationship between external forces applied to cell-matrix adhesions and their state of aggregation: applying force by optical tweezers (Choquet et al., 1997) or micropipette manipulation (Riveline et al., 2001) stimulates signaling from and growth of FAs. Recently, we have found that for stationary cells there is a linear relationship between the internal forces exerted at a FA and its lateral size (Balaban et al., 2001). Another recent study has shown that this relationship is inverse for focal complexes close to the advancing edge of locomoting fibroblasts (Beningo et al., 2001).

Until recently, quantitative measurements of force have been hardly possible on the level of FAs, in contrast to the level of single molecules, which have been investigated extensively with a variety of quantitative methods, including optical tweezers (Finer et al., 1994), atomic force microscopy (Rief et al., 1997), and the biomembrane force probe (Merkel et al., 1999). The main technique to measure cellular forces is the elastic substrate method (Beningo and Wang, 2002), which was introduced by Harris and coworkers in the early 1980s (Harris et al., 1980, 1981). Until today, there are few alternative methods to the elastic substrate method. One of them is the use of a micromachined device, that measures cellular forces acting on cantilevers etched into a solid substrate (Galbraith and Sheetz, 1997); another is the use of centrifugal forces to induce rupture of adhesion (Thoumine et al., 1996).

In the seminal work by Harris and coworkers (Harris et al., 1980, 1981), the highly viscous, polymeric fluid polydimethylsiloxane (PDMS) was crosslinked at the surface by exposing it to heat. A thin elastic film over a fluid is obtained that under cell traction yields a wrinkled pattern, which is

characteristic of the pattern of forces exerted. Major improvements of the wrinkling substrates method include the tuning of the elastic compliance (Burton and Taylor, 1997; Burton et al., 1999). However, deformation data can be analyzed only semiquantitatively with this technique, because the buckling of thin polymer films is a nonlinear phenomenon that is very difficult to treat in elasticity theory. Wrinkling can be suppressed by prestressing the film, thus allowing only for tangential deformation, which can be tracked by fluorescent latex beads (Lee et al., 1994). Quantitative analysis of elastic substrate data was pioneered by Dembo and coworkers. Using linear elasticity theory for thin elastic films and numerical algorithms for solving inverse problems, the forces exerted by keratocytes on the substrate could be reconstructed (Dembo et al., 1996; Oliver et al., 1999). One key ingredient of this method is the use of a regularization scheme, because the inverse problem is ill-posed (that means highly sensitive to noise in the displacement data).

For strong mammalian cells like fibroblasts, the nonwrinkling PDMS-films are too weak. By replacing PDMS with polyacrylamide (PAA) gel, a thick elastic substrate was achieved, which is soft enough to deform under cell traction (Pelham and Wang, 1997). Like any isotropic elastic medium, it is characterized by two elastic constants. In several recent studies, a thick PAA film with Young modulus $E \approx$ 6 to 24 kPa and Poisson ratio $v \approx 0.5$ was used to quantitatively investigate traction of fibroblasts (Dembo and Wang, 1999; Lo et al., 2000; Beningo et al., 2001). Because the marker bead displacements near the substrate surface are much smaller than the film thickness, they can be evaluated under the assumption that the thick film behaves like an elastic halfspace, whose elastic Green function is well known (Landau and Lifshitz, 1970). This allowed to reconstruct a continuous force field emanating from underneath the cell by using standard techniques for the solution of ill-posed inverse problems. Very recently, is has been suggested by Butler and coworkers that the inverse problem becomes computationally more efficient when being solved in Fourier space and that regularization is not needed when reconstructing the force pattern (Butler et al., 2002).

Recently, we developed a novel elastic substrate technique to measure cellular forces at the level of single FAs (Balaban et al., 2001). A thick polymer film made from PDMS with a Young modulus $E \approx 10$ to 20 kPa and Poisson ratio $v \approx 0.5$ was micropatterned by standard lithographic techniques. Due to the regularity of the surface pattern, its deformation can be easily extracted from microscope pictures by an automatic procedure. Cell traction was generated by stationary, yet mechanically active cells (human foreskin fibroblasts, cardiac fibroblasts, or cardiac myocytes) expressing green fluorescent protein (GFP)-vinculin. Vinculin is one of the major proteins of the submembrane plaque of FAs and can be tagged with GFP at its amino terminal. GFP-vinculin localizes at FAs and has good overlap with the dark areas in interference reflection microscopy (Riveline et al., 2001). In our setup, GFP-vinculin marks FAs with very high optical quality. The cells studied in our experiments show mature adhesion with well-developed FAs and stress fibers and with little ruffling activity. We never observed traction near an area deprived of FAs, which allows us to assume that FAs are the main sites of application of force by the cells and to develop a numerical procedure, which reconstructs discrete forces at sites of FA. Correlation with the lateral size of the FAs showed that there exists the following linear relationship between force F and area A of a single FA: $A \approx 1 \ \mu m^2 + 0.2 \ \mu m^2/nN \ F$. In detail, we found a stress constant of $5.5 \pm 2 \ nN/\mu m^2$. For close packing of integrins, this finding translates into a force of few pN per receptor, which is consistent with recent experiments on strength of single molecular bonds at slow loading (Merkel et al., 1999).

The main difference between our new method and previous work on force reconstruction on thick elastic substrates (Dembo and Wang, 1999; Lo et al., 2000; Beningo et al., 2001) is the assumption of localized force, which necessitates several changes to the standard procedure. In this paper, we address the details of our new computational method and show how the elastic substrate method is affected by the assumption of localized force and the need for regularization. We use systematic simulation of data to confirm that the inverse problem of linear elasticity theory is ill-posed for reasonable levels of noise and to show that regularization in general cannot be neglected. Data simulation is also used to estimate both the spatial and force resolution of our method. The concept of a force multipolar expansion is used to show under which experimental conditions one can neglect the details of the force distribution close to FAs and the finite thickness of the elastic substrate.

MATERIALS AND METHODS

Experimental method

The details of the experimental method have been described previously (Balaban et al., 2001). Briefly, the preparation of the micropatterned surfaces was carried out in two steps. First, the negative pattern (typically a grid of 0.5-μm diameter dots with pitch 2 μm) was prepared using standard optical lithography on solid substrates (Si or GaAs wafers). The solid substrates and their photoresist (Microposit S1805, Shipley) pattern were then used as a mold for patterning the surface of the PDMS elastomer. The PDMS elastomer (Sylgard 184, Dow Corning) was poured on glass coverslips, partially cured, put in contact with the photoresist molds, and cured again. After peeling off the mold, the photoresist pattern resulted in a topographic modulation of 0.3-μm depth on the surface of the 40-μm-thick PDMS layer. The topographic pattern was visualized with phase-contrast microscopy. Alternatively, pretreatment of the mold resulted in a fluorescent pattern, which was peeled off with and remained in the elastomer, which then has no topographic modulation.

The bulk elastomer was characterized by suspending known masses to the end of stripes, as described by Pelham and Wang (1997). The elastomer stripes return to their original length even after applying a force that induces an elongation of 70% for 24 h. The Poisson ratio was found to be $v \approx 0.5$, by following changes in volume upon stretching. The Young modulus varied

between 12 to 1000 kPa, as the ratio of the silicone elastomer to curing agent varied from 50:1 to 10:1. Note that a Young modulus of 1 kPa is considerably less than the value for houseware rubber, which is 1 MPa. In a simple scaling picture the Young modulus is $kTc = kT/a^3$, in which c is the effective crosslinker concentration and a is the effective mesh size. Thus, a difference of three orders of magnitude in Young modulus E corresponds only to a difference of one order of magnitude for mesh size a (from 1.6 nm to 16 nm for a change in E from MPa to kPa).

Additional calibration of the surface properties was performed in situ under the microscope: the patterned elastomer surfaces were immersed in culture medium for several days and a calibrated micropipette was used to deflect the surface. The deflection of the micropipette was measured and translated into force. Knowing the force applied by the calibrated micropipette, the Young modulus of the elastomer was calculated from the displacements as described below and found to be consistent with the value measured in the bulk. The relaxation time of the patterned elastomer after mechanical perturbation was measured by phase contrast microscopy, using a video system (25 frames/s). The typical time for rapid recoiling to 80% of the distance to the original position was 100 ms, whereas full relaxation (>95%) occurred within 400 ms.

Before plating, the substrates were coated with fibronectin. Cells (human foreskin fibroblasts, cardiac fibroblasts, or cardiac myocytes) from primary cultures were transfected with GFP-vinculin and plated on the substrates. Observation was done between 10 to 60 h after plating. Image acquisition was done as previously described using the DeltaVision acquisition system (Applied Precision, Issaquah, WA) (Zamir et al., 1999, 2000). Images were processed with Priism software.

Computational method

Linear elasticity theory

For adhesion onto a planar substrate, cultured cells usually adopt a flat morphology and cell traction is exerted onto the surface in a way that is essentially tangential. Therefore, the force vectors can be assumed to be two-dimensional in the plane of the substrate surface. Our substrates are isotropic elastomers. Thus, they are characterized by two elastic constants, Young modulus E and Poisson ratio v. They are also incompressible, that is the Poisson ratio v is close to 0.5. The Young modulus E is between 10 and 20 kPa, which under typical cell traction leads to displacements of the order of 1 μm. Because this is much smaller than the polymer film thickness of 40 μm, the substrate can be considered to be an elastic isotropic halfspace (see below for a more detailed discussion of finite size effects).

In the framework of linear elasticity theory, stress field $F(r)$ and displacement field $u(r)$ are related by a Fredholm integral equation of the first kind:

$$u_i(r) = \int dr' G_{ij}(r - r')F_j(r') \quad (1)$$

in which we apply the summation convention. In general, one has $1 \le i$, $j \le 3$. In our case, G_{ij} is the Green function of the elastic isotropic halfspace, which was calculated in the 19th century by Boussinesq (Landau and Lifshitz, 1970). The Boussinesq solution implies that for tangential traction and Poisson ratio $v = 0.5$, there is no out of plane displacement. Because our substrates have Poisson ratio v close to 0.5, we can assume

that the displacement vectors are two-dimensional in the x-y plane. Therefore, the whole elastic problem is two-dimensional, $1 \le i, j \le 2$. The Green function for the surface displacements for Poisson ratio $v = 0.5$ is

$$G_{ij}(r) = \frac{3}{4\pi Er}\left(\delta_{ij} + \frac{x_i x_j}{r^2}\right) \quad (2)$$

with $r = |r|$ and δ_{ij} the Kronecker Delta. For a given traction pattern $F(r)$, the surface displacement $u(r)$ follows from using Eq. 2 in Eq. 1. Note that the Green function is long ranged (it scales inversely with distance) and scales inversely with Young modulus E. The displacement following from a point force F scales as $u = l(l/r)$ with distance r, in which $l = \sqrt{F/E}$ is the length set by force and rigidity. Therefore l is a measure both for typical displacements and for the decay length of elastic effects. As can be seen from the data presented below, we always have $|du/dr| \ll 1$, thus linear elasticity theory is valid.

Inverse problem

In the case of topographically structured substrates, the displacement field $u(r)$ is measured at different sites r_i ($1 \le i \le N$) by image analysis of the phase contrast image (in the case of fluorescently structured substrates, the fluorescence image was used). For this purpose we use the water algorithm, which has been described elsewhere (Zamir et al., 1999). To quantify the error related to the automatic determination of the centers of the spots, we used the water algorithm several times on the same picture to determine the positions of the grid. The standard deviation was found to be of the order of 1 pixel (0.133 μm). The same result was found when subtracting the displacement following from reconstructed force patterns from the experimentally measured displacement. The inverse problem of calculating forces from displacements amounts to inverting the Fredholm equation of the first kind from Eq. 1. However, this is not an easy task, because this kind of Fredholm integral equations and their discretizations are ill-posed. A problem is called ill-posed if its solution is not unique or if it is not a continuous function of the data. Fredholm integral equations of the first kind and their discretizations are ill-posed because they constitute smoothing operations, which remove high-frequency components. Inverting the smoothing operation from Eq. 1 is an underdetermined problem (too much information has been lost during smoothing), which causes the solution F to be very sensitive to any change in u. Ill-posed inverse problem can be solved by regularization, that is by including additional information that stabilizes the solution. They are a subject well investigated in numerical mathematics, and a number of regularization schemes are available for their solution (Press et al., 1992; Hansen, 1998).

We approximate the cellular force pattern by an ensemble of point-like forces localized to the sites of focal adhesion (see below for a detailed discussion of this approximation). The different positions r_i ($1 \le i \le M$) of the different focal contacts can be reconstructed from the fluorescence image with the water algorithm (Zamir et al., 1999). As will be argued below, we can assume that each focal contact corresponds to a point force F_i as long as we take care not to include displacements that are closer to a FA than its lateral extension. Because both forces and displacements are at discrete positions, the integral equation from Eq. 1 now becomes a set of linear equations, $u = GF$, in which $u = (u_1(r_1), u_2(r_1), u_1(r_2), u_2(r_2), \ldots)$ is a $2N$-vector, $F = (F_1(r_1'), F_2(r_1'), F_1(r_2'), F_2(r_2'), \ldots)$ a $2M$-vector and G the following $2N \times 2M$-matrix:

$$\begin{pmatrix} G_{11}(r_1 - r_1') & G_{12}(r_1 - r_1') & G_{11}(r_1 - r_2') & G_{12}(r_1 - r_2') & \cdots \\ G_{21}(r_1 - r_1') & G_{22}(r_1 - r_1') & G_{11}(r_1 - r_2') & G_{12}(r_1 - r_2') & \cdots \\ G_{11}(r_2 - r_1') & G_{12}(r_2 - r_1') & G_{11}(r_2 - r_2') & G_{12}(r_2 - r_2') & \cdots \\ G_{21}(r_2 - r_1') & G_{22}(r_2 - r_1') & G_{11}(r_2 - r_2') & G_{12}(r_2 - r_2') & \cdots \\ \vdots & \vdots & \vdots & \vdots & \ddots \end{pmatrix} \quad (3)$$

Each experiment gives a displacement vector $u \in R^{2N}$ and a Green matrix $G \in R^{2N \times 2M}$, which can be used to solve the inverse problem, which is to find the force vector $F \in R^{2M}$. We use the usual χ^2-estimate, that is the quality of the estimate is measured by the sum of least squares $\chi^2 = |GF - u|^2/\sigma^2$ (Press et al., 1992). Here σ is the standard deviation of the distribution of measurement errors for the vector components of the displacement u. χ^2-estimates are known to be useful even if the measurement errors are not normally distributed. Here we assume that this distribution is normal with the same standard deviation σ for each component of u. Then the quantity χ^2 is drawn from a χ^2-distribution with $2(N - M)$ degrees of freedom, which is χ^2 has an average $2(N - M)$ and a standard deviation $\sqrt{4(N - M)}$.

In principle, the set of linear equations $u = GF$ can be solved by singular value decomposition. However, this procedure will in general not lead to reasonable results, because the problem at hand is ill-posed. This means that the singular values of the matrix G decay gradually to cero, thus the matrix G is ill-conditioned (in our analysis, condition numbers of the order of 1000 are typical). Following the usual procedure for discrete ill-posed inverse problems (Press et al., 1992; Hansen, 1998), we now add a side constraint to the χ^2-minimization, which in itself is not ill-posed and ensures a solution F that is robust. In more physical terms, the procedure aims at filtering out the parts of the displacement data that are due to noise. In the framework of Bayesian theory, the additional constraint is an a priori hypothesis about the physical nature of the expected solution. Below, we will use simulated data to show that in the presence of noise, a regularization scheme is an indispensable part of force reconstruction from elastic substrate deformations.

The need for regularization necessitates two choices: which side constraint should be chosen to stabilize the inversion procedure and how strongly this side constraint is enforced for each set of experimental data. The choice of the side constraint should be guided by physical considerations. The simplest choice is zero-order Tikhonov regularization, where one minimizes χ^2 under the constraint that the forces should not become exceedingly large:

$$\min_F \{|GF - u|^2 + \lambda^2 |F|^2\}. \quad (4)$$

The Lagrange parameter λ is called the *regularization parameter* because it parametrizes the trade-off curve between agreement with the given data (first term) and regularization (second term). For zero-order Tikhonov regularization, λ essentially determines below which level contributions from small singular values are filtered out of the solution. First and higher order regularization involves derivatives of F and should be chosen for enforcing smooth force fields. However, because neighboring focal adhesions can connect to different stress fibers, which might point in different directions, there is no reason to assume smooth force fields. Zero-order regularization both leads to a simple protocol for the numerical analysis and is the most reasonable choice in our case. The new target function is still quadratic in u and therefore again can be solved by singular value decomposition. For this numerical work, we used the package of Matlab routines *Regularization Tools* by P. C. Hansen. It can be found at Netlib (http://www.netlib.org/) in the file numeralgo/na4. Detailed explanations are provided in the book by the same author (Hansen, 1998).

To choose the regularization parameter λ, we have used the χ-criterion (Press et al., 1992) and the *L*-curve criterion (Hansen, 1998). The χ-criterion (also known as *discrepancy principle*) suggests that λ is chosen in such a way that the residual norm $R = |GF - u|^2$ as a function of λ assumes the value expected for an optimal fit, $2(N - M)\sigma^2$. The *L*-curve criterion suggests to determine the value of λ at which the residual norm starts to increase significantly as a function of λ. The name of this criterion comes from the fact that for discrete ill-posed problems, a plot of $\log |F|^2$ versus $\log |GF - u|^2$ very often has a L shape. The corner of the L curve corresponds to the optimal balance between data agreement and regularization, and it is this corner (which is intrinsic to the data at hand), which we detect with the *L*-curve criterion. One disadvantage of this method is that it introduces the need for a corner-finding algorithm. Another potential choice is the self-consistence criterion (Honerkamp and Weese, 1990),

which suggests that the regularization parameter λ is chosen in such a way that the resulting force pattern can be used to simulate displacement data, which is consistent with the original set of data. Although this criterion is computationally expensive, the notion of self-consistence is very helpful in general. In particular, if σ is the standard deviation of the noise in the experimental data, then λ should be chosen sufficiently small that the standard deviation between experimental and reconstructed displacement equals σ.

Resolution and bootstrap method

In general, there is no easy way to estimate our resolution, so we used simulated data to do so. The main problem is spatial resolution of the force field, because the kernel of the Fredholm integral equation smoothes out the force field on the length scale $\sqrt{F/E}$. Thus, for force F on the nN-scale and Young modulus E on the kPa-scale, the spatial resolution of our method cannot be below the micrometer scale. Therefore, force estimates can be attributed to single FAs only if they are farer apart from each other than a few micrometers. However, the exact value depends on the details of the force pattern and the amount of noise in the experimental data. There are several possible reasons for statistical error in our data. They include limitations due to the microscope setup, anisotropic illumination of the image field, uncertainty in the detection of spatial positions with the help of the water algorithm, and possible shifts between the coordinate systems in which the marker positions are determined with and without cell traction.

The spatial and force resolutions of our technique will be derived below by simulating displacement data from artificial force patterns. For this analysis we assume that Gaussian noise adds to the vector components of the displacement field u with a standard deviation σ. The use of simulated data is a very powerful tool. In particular, it allows to derive confidence intervals for given data sets (bootstrap method) and to determine the regularization parameter λ (when using the self-consistence criterion). The bootstrap method is a computational method to calculate statistical accuracy by data resampling (Press et al., 1992; Efron and Tibshirani, 1993). First a force estimate is obtained as explained above. Then many sets of displacement data are simulated on the basis of this force pattern. For each new data set, the inverse problem is solved. Finally the experimental standard deviation is identified with the standard deviation of the different force estimates.

Force distribution at focal adhesions

The lateral extension of FAs ranges up to few micrometers and can be visualized by GFP-labeling of FA-proteins like vinculin or paxillin. Initial and mature FAs are dot- and streak-like, respectively. In most cases, their shape resembles an ellipse with half axes a and b. Force is distributed over this area in a way that in general is unknown. However, as the distance to the force bearing region increases, details of the force distribution become less relevant for the determination of the displacement field. This is analogous to electrostatics, where the far field potential produced by a compact charge distribution is determined essentially by its highest multipole moment. In fact, the concept of a multipolar expansion can also be applied to elasticity theory. By expanding Eq. 1 for distances larger than the lateral extension of the force distribution, we find for the displacement field

$$u_i(r) = \sum_{n=0}^{\infty} \frac{(-1)^n}{n!} \frac{\partial}{\partial x_{i_1}} \cdots \frac{\partial}{\partial x_{i_n}} G_{ij}(r - r') P_{i_1 \ldots i_n j} \quad (5)$$

in which r' is some suitably defined midpoint of the force bearing region and the $P_{i_1 \ldots i_n i}$ are its force multipoles

$$P_{i_1 \ldots i_n i} = \int ds_{i_1} \ldots s_{i_n} f_i(r' + s). \quad (6)$$

The force monopole P_i is a vector that describes the overall force exerted from the force bearing region, and the force dipole P_{ij} is a second-rank tensor that describes pinch-like contractions or expansions. It follows from Eq. 2 that the displacements caused by force monopoles and force dipoles decay with distance like $1/r$ and $1/r^2$, respectively. The next term in the expansion of Eq. 5 is the force quadrupole P_{ijk}, that is a tensor of rank 3, which decays like $1/r^3$.

The major assumption of our numerical analysis will be that forces are exerted mainly at FAs and that the distributed force close to each FA can be approximated by its first multipole moment, the force monopole, or overall force. To justify the mathematical part of this assumption, we consider the following microscopic model for the force distribution over a FA. First, we assume that all of the distributed force is directed in the same direction. Second, we assume that the distribution of magnitude of force is Hertzian. This means that the force disappears continuously towards the rim and reaches its maximum in the middle. If we choose the x axis to be the a axis of the FA, we can write

$$F(x, y) = \frac{3}{2\pi ab} \sqrt{1 - \left(\frac{x}{a}\right)^2 - \left(\frac{y}{b}\right)^2} F_0. \qquad (7)$$

The corresponding force multipoles follow from Eq. 6. The force monopole $P = F_0$, the force dipole P_{ij} vanishes, and the force quadrupole has $P_{11i} = a^2 F_{0,i}/5$, $P_{22i} = b^2 F_{0,i}/5$ and vanishes otherwise.

We now consider how the displacement decays along the x and y axes for a force in x direction; in these high symmetry directions, the displacement vector has a contribution only in x direction, but it is easy to check that the following results also hold for arbitrary directions. For the monopole of our model, it follows from Eq. 5 that the displacement decays like $3F_0/2\pi Er$ along the x axis and like $3F_0/4\pi Er$ (that is twice as fast) along the y axis, respectively. For the quadrupole of our model, it follows from Eq. 5 that the displacement decays like $3F_0(a^2 - b^2)/10\pi Er^3$ along the x axis and like $3F_0(a^2 + 2b^2)/40\pi Er^3$ along the y axis, respectively. For a symmetric FA, $a = b$, the contribution from the quadrupole vanishes along the x axis. Along the y axis, it becomes smaller than the contribution from the monopole for $r > \sqrt{3/10}a$. In general, a and b set the length scales over which the corrections to the monopole contribution become negligible. Thus, we can expect the crossover between the displacement following from the distributed force and the displacement following from the force monopole to occur close to the rim of the FA, at a distance that is set by the size of the FA itself.

For our model force distribution, this conclusion can be checked numerically by using Eq. 2 and Eq. 7 in Eq. 1. In Fig. 1, we compare the full and approximate displacements (dashed and solid lines, respectively) for distributed force being directed parallel (left column, A–C) and perpendicular (right column, D–F) to the FA elongation. Note that in contrast to the displacement due to the point-like force monopole, the displacement due to the distributed force does not diverge at the origin (in fact it scales like F_0/Ea). As predicted from our multipole argument, it crosses over to the full solution (which scales like F_0/Er) close to the rim of the force-bearing region. In Fig. 1, b and e, the magnitude of displacement is plotted along the x axis, and in Fig. 1, c and F, along the y axis. In all cases, the crossover between full and approximate solutions occurs very rapidly outside the force-bearing regions, especially if the direction of force is parallel to the elongation of the focal adhesion. We conclude that as long as one does not consider displacements, which are closer to a FA than the size of the FA itself, the divergence of the Green function is avoided and it is justified to approximate the distributed force exerted at an FA by a point force.

Finite size effects

In our experiments, we used polymer films with thickness 40 μm and lateral size of a few centimeters. Typical displacements used during quantitative analysis were of the order of $\sqrt{F/E} \approx \mu$m, in which $F = 10$ nN is the typical force at FAs and $E = 10$ kPa a typical value for the Young

modulus. We now argue in more detail why finite size effects can be neglected in our treatment. In linear elasticity theory, forces, and displacements are related by a second order differential equation. For a given force distribution, one first solves the heterogeneous differential equation for an infinite elastic medium. The resulting solution will be an inverse power of the distance and it will not be unique, because any solution to the homogeneous differential equation could be added to it. These additional solutions are called image displacements and will be polynominals in the distance. They can be used to satisfy the boundary conditions of the finite sized sample. For free and clamped surfaces, forces normal to the boundary and displacements have to vanish at the boundaries, respectively.

The Boussinesq Green function for an infinite elastic half-space is used throughout our work, although in principle one should use the Green function, which also satisfies the clamped boundary conditions at the bottom and at the sides of the thick film. This Green function will be very complicated, but one can estimate its effect as follows. Consider one FA with overall force F. Then the displacement at a distance r scales as $u = F/Er$, whereas the image displacement scales as $u = cr$, where c is a dimensionless factor that has to be determined from the boundary conditions. For clamped boundary conditions, the two displacements have to cancel at $r = h$, in which h is film thickness (a similar argument applies for the sides of the sample). Therefore, $c = F/Eh^2 = (l/h)^2$, in which $l = \sqrt{F/E}$ is the length scale set by forces and rigidity. Because l is also the length scale for displacements close to the FAs, c is negligible if displacements are much smaller than film thickness, as it is usually the case in elastic substrate experiments with thick films.

As explained in the preceding section, the displacement at the position of the FA itself scales as F/Ea, in which a is the size of the FA. If film thickness h decreases towards a, this scaling is changed to Fh/Ea^2 and our treatment is not valid anymore, because we neglect the effect of finite film size. Therefore, an additional requirement for our method is that the size of FAs (or of a cluster of neighboring FAs if the corresponding forces point in the same direction) should be much smaller than the film thickness. Butler and coworkers recently used the same scaling argument to argue that cell size should be much smaller than film thickness, because they considered the case that stress is distributed uniformly over the whole cell (Butler et al., 2002). However, in our analysis forces at different FAs (or at least at FAs in different parts of the cell) had different directions and therefore screen each other. To consider the effect of the whole cell, one should take at least into account that the vector sum of all forces will vanish due to Newton's third law. In the framework of the force multipolar expansion, the relevant term becomes the force dipole, and in fact force patterns from mechanically active cells often resemble pinching deformations. Below we analyze an experiment that shows that stationary fibroblasts might be considered to generate force dipoles of magnitude $P = -10^{-11}$ J (see Cell traction). Then displacement decays as $u = P/Er^2$ and $c = P/Eh^3 = (l/h)^3$, in which now $l = (P/E)^{1/3} \approx 10$ μm is the length scale set by force dipole and rigidity. Therefore, the additional requirement now becomes that the length scale set by force dipole and rigidity should be much smaller than film thickness. Although both additional requirements discussed in this paragraph are somehow stronger than the usual one derived in the preceding paragraph, they are less drastic than the one suggested by Butler and coworkers and usually are satisfied in elastic substrate experiments with thick films.

As explained above, the micropatterning of the elastic substrates was realized either by topographic or fluorescent modulation. In both cases, corrections arise to the ideal case of an infinite halfspace, as hollow and stiff inclusions, respectively, decorate the upper side of the elastic substrate. Here we neglect these corrections because the inclusions are not larger than the length scale $\sqrt{F/E} \approx \mu$m set by forces and rigidity. For future work, one might consider decreasing the size of the surface pattern, e.g., by using nonlithographic techniques. Note that the same beneficial effect of the smoothing action also applies to the conventional work with marker beads, which also give rise to corrections to the Boussinesq Green function.
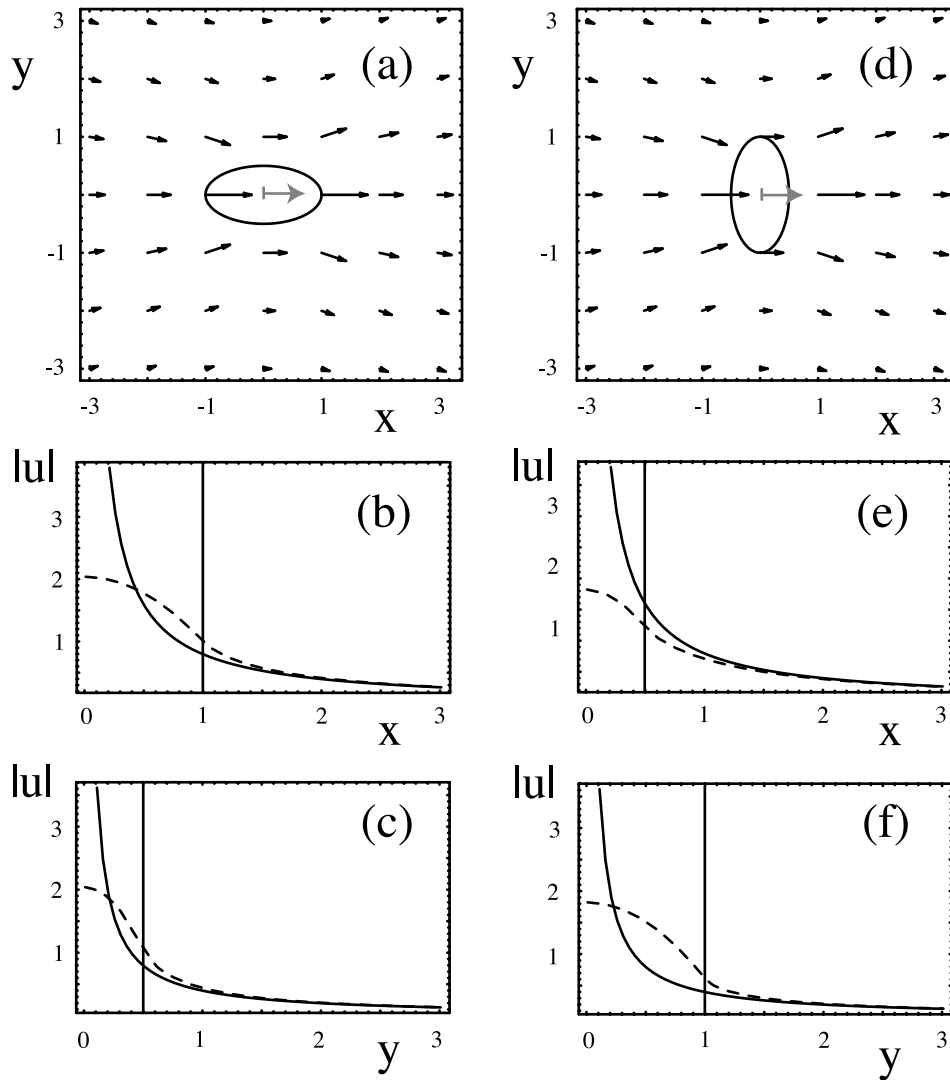
FIGURE 1 Theoretical model for force distribution over a finite-sized adhesion plaque like a focal adhesion: we assume that force points in *x* direction and that its magnitude is distributed in a Hertzian manner over an ellipse. (*a*, *b*, and *c*) Long axis of ellipse parallel to direction of force. (*d*, *e*, and *f*) Long axis of ellipse perpendicular to direction of force. (*a* and *d*). Displacement following from the distributed force. (*b*, *c*, *e*, and *f*) Dashed lines: magnitude of displacement following from the distributed force along the *x* and *y* directions (numerical result). Solid lines: magnitude of displacement following from equivalent point-like forces exerted at the origin (Boussinesq Green function). Vertical bars mark the edge of the focal adhesion. For Young modulus $E = 6$ kPa and overall force $F = 10$ nN, all distances are in micrometers. The crossover from the distributed description to the point-like description occurs outside the focal adhesion boundaries on the scale of the ellipse dimensions.

RESULTS

Simulated data

Data simulation allows an accurate check of our method and to estimate its resolution. In Fig. 2 *a* we show an artificial force pattern F_0 that mimics traction by a polarized fibroblast as monitored in our experiments. The cell is assumed to be elongated with FAs occuring close to the rim. Forces are assumed to be exerted only at the FAs at the lower and upper sides, which can be considered to be connected by stress fibers running parallel to the long axis of the cell. One test of our force reconstruction will be whether forces are

generated at the focals at the sides, which in the original pattern do not exert force. Neighboring forces along the upper and lower sides are separated by a distance of 4 μm and are assumed to alternate in magnitude, because this allows to test the resolution of our force reconstruction. Typical force is assumed to be 20 nN per FA. Fig. 2 *a* also shows the displacement resulting from this force pattern. The relation between force and displacement is governed by the Young modulus *E*, which we assume to be 12 kPa (this is the smallest value obtained in our experiments). Displacements are calculated on a grid of dots with pitch 2 μm (like for the micropatterned substrates) and are assumed to be
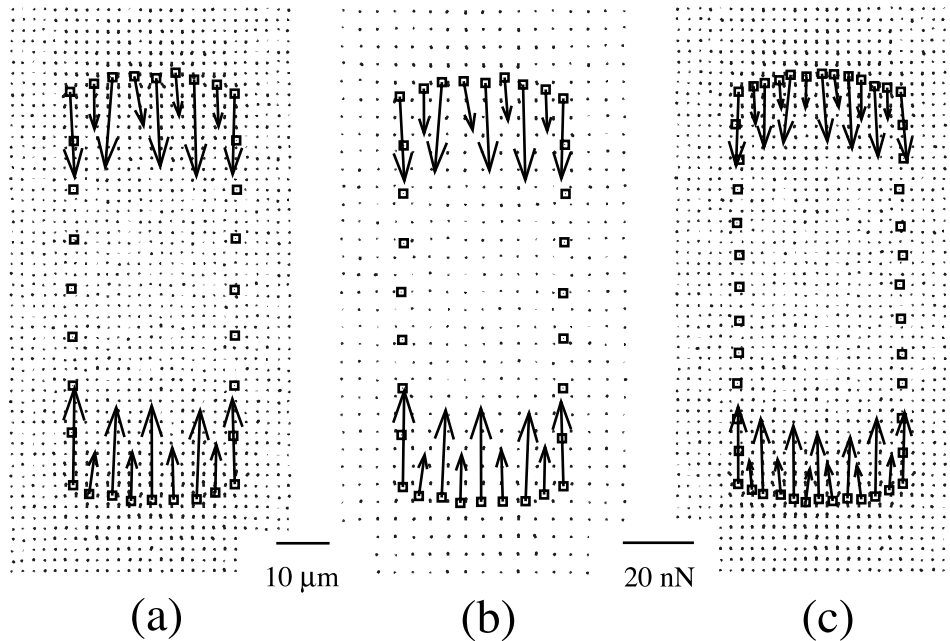
FIGURE 2   Artificial force patterns F_0 mimicking traction by polarized fibroblasts and the resulting displacement fields u. We assume that focal adhesions form a rim, but forces are exerted only at the upper and lower sides. Force magnitude is alternating to test the resolution of the force reconstruction. The assumed Young modulus is $E = 12$ kPa. (*a*) Nine focals adhesions on each side with average distance 4 μm. The distance between the microfabricated dots is 2 μm. Typical magnitude of force is 20 nN. Displacement is subject to Gaussian noise with standard deviation $\sigma = 1$ pixel $= 0.133$ μm, largest displacement is 1.3 μm. (*b*) Same parameter values as in *a*, but doubled distance between the micro-fabricated dots. (*c*) Same parameter values as in *a*, but now there are 13 focal adhesions with distance 2 μm on each side. Typical force has been slightly decreased as to achieve same maximal displacement.

subject to Gaussian noise with standard deviation $\sigma = 1$ pixel $= 0.133$ μm (this is the level of noise resulting from image processing with the water algorithm). Then the largest displacement picked up is 1.3 μm. Fig. 2, *b* and *c*, show two of the several changes to this reference case that we will discuss below: in Fig. 2 *b*, the distance between microfabricated dots has been increased from 2 to 4 μm, and in Fig. 2 *c*, the number of FAs has been increased from 9 to 13 (thus, the distance between FAs has been decreased from 4 to 2 μm).

In Fig. 3, we reconstruct the force pattern from the displacement data shown in Fig. 2 *a*. In Fig. 3 *a*, we plot residual norm $R = \left| GF(\lambda) - u \right|^2$ (in absolute units) and deviation from original force $\Delta F = \left| F(\lambda) - F_0 \right|$ (normalized to 100) as a function of regularization parameter λ. For small regularization (small λ), maximal agreement with the data is achieved; the residual norm R nevertheless attains a finite value, because there is no force field that can exactly reproduce the displacements due to Gaussian noise. For large regularization (large λ), the force field vanishes and the residual norm levels off at the value $|u|^2$. The solid and dotted straight lines indicate expectation value and confidence interval, respectively, for a χ^2 estimate. Its intersection with the R curve suggests $\lambda = 0.04$ for the regularization. In fact this is also the value of λ for which R starts to rise as a function of λ, so this result agrees nicely with the *L*-curve criterion. More important, it also agrees with the

minimum in ΔF, the deviation from the original force pattern. It is important to note that even the optimal choice of λ cannot reproduce the original force pattern. Fig. 3 *a* shows that ΔF has its minimum at 24%, that means a considerable part of the original information has been lost by the smoothing operation of the elastic kernel and cannot be retrieved by the inversion. This corresponds to a error of 4 nN for the reconstruction of the 20 nN original single force. The fact that ΔF rises again for smaller values of λ indicates the need for regularization: without regularization ($\lambda = 0$, $\Delta F = 30\%$), the agreement between reconstructed and original force is worse than for the proper value of regularization ($\lambda = 0.04$, $\Delta F = 24\%$). In Fig. 3 *b* we plot the reconstructed (solid) and original (dashed) force pattern. Note that our method nicely reproduced the overall characteristics of the pattern: only small forces are generated at the sides, and for the forces at the upper and lower sides, both the directions and the alternating magnitudes are reproduced. In Fig. 3 *c*, we show an example of larger regularization ($\lambda = 0.1$), which is still within the χ^2-interval and consistent with a noise level of $\sigma = 1$ pixel $= 0.133$ μm. Yet the resolution in the force magnitude is lost, and their values are estimated as being too low.

Until now we showed that for parameter values corresponding to our experiments, the spatial resolution can be considered to be better than 4 μm and the force resolution will be around 4 nN. We now demonstrate that for data
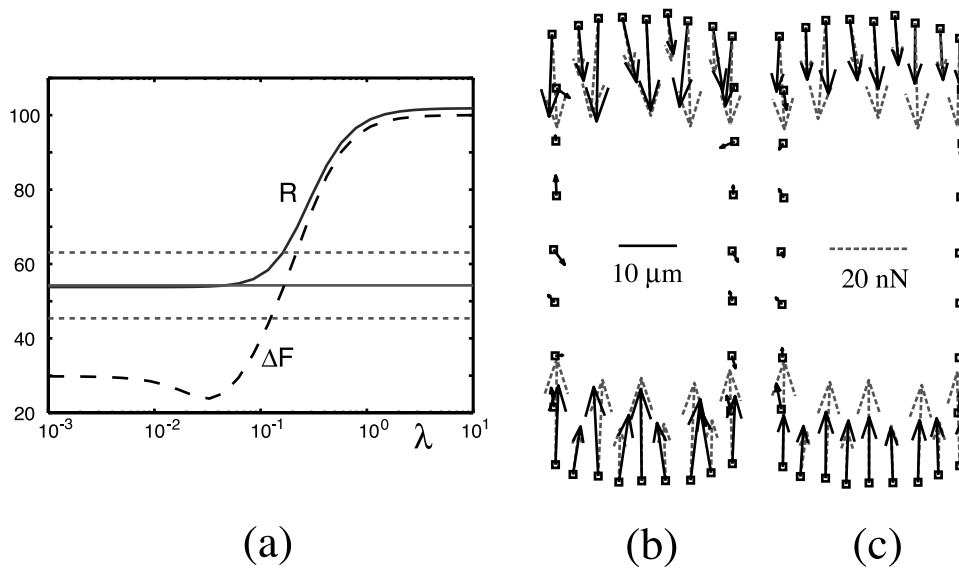
FIGURE 3   (*a*) Residual norm $R = |GF(\lambda) - u|^2$ (in absolute units) and deviation from original force $\Delta F = |F(\lambda) - F_0|$ (normalized to 100) as a function of regularization parameter λ for the force and displacement data from Fig. 2 *a*. The solid and dotted straight lines indicate expectation value and confidence interval for the corresponding χ^2-estimate, respectively. For the choice of the regularization parameter λ, χ^2-criterion, *L*-curve criterion and the minimum in ΔF all suggest $\lambda = 0.04$. (*b* and *c*) Dashed and solid arrows are original and reconstructed forces, respectively. (*b*) Force reconstruction with $\lambda = 0.04$. Even for optimal reconstruction, some information is inevitably lost. (*c*) Force reconstruction with $\lambda = 0.1$. Regularization is too strong and spatial resolution is lost.

containing less information than assumed here, force reconstruction will worsen considerably. In Fig. 4, we show the effect of a noise level increased to $\sigma = 2$ pixel $= 0.266$ μm. Monitoring R and ΔF as a function of λ (Fig. 4 *a*) determines $\lambda = 0.09$ for optimal regularization, but this time ΔF is considerably higher (37% compared with 24%), and goes up to 60% for the case without regularization (compared with 30% for the reference case). As was to be expected,

with increased noise, regularization becomes more relevant. Fig. 4, *b* and *c*, compare reconstructed and original force patterns for $\lambda = 0.09$ and vanishing λ, respectively. In the first case of optimal regularization, force reconstruction is worse than in Fig. 3 *b* for less noise, and in the second case without regularization, the force pattern becomes rather erratic. In particular, now larger forces are generated at the sides.
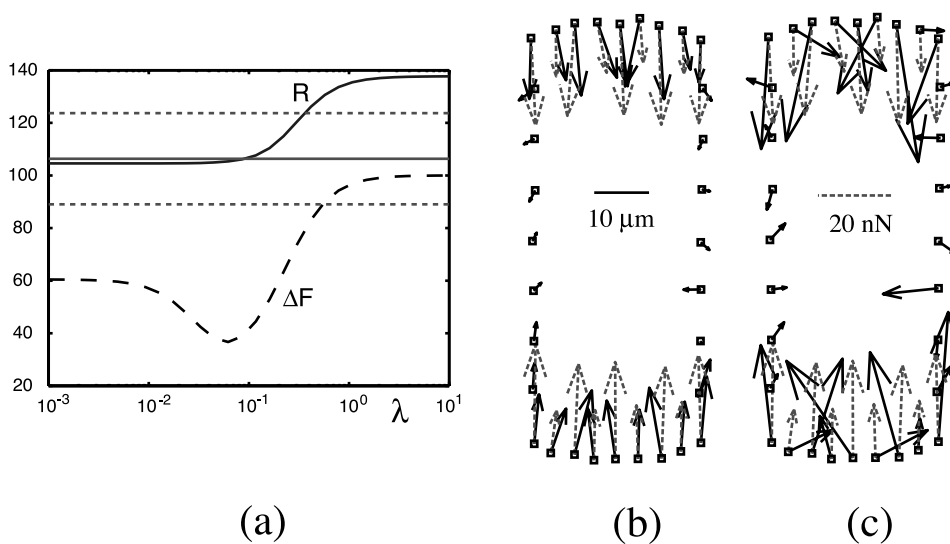

FIGURE 4   (*a*) Residual norm R and deviation from original force ΔF as a function of regularization parameter λ for the force pattern from Fig. 2 *a* with the noise level increased to $\sigma = 2$ pixel $= 0.266$ μm. (*b*) Force reconstruction with $\lambda = 0.09$. Due to larger noise, more information is lost even for optimal regularization. (*c*) Force reconstruction without regularization ($\lambda = 0$) yields a rather erratic force pattern.
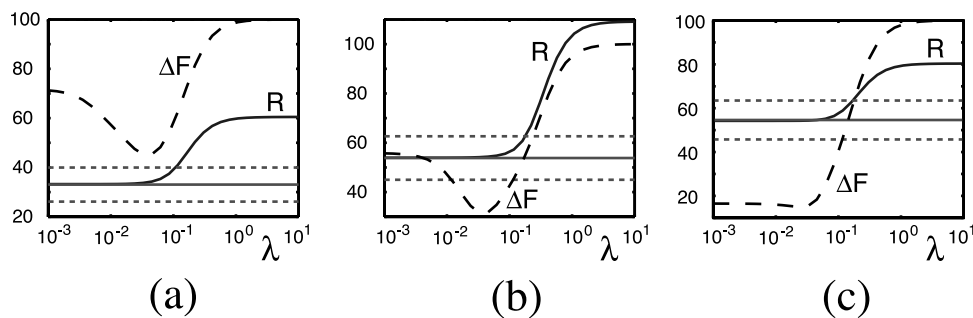
FIGURE 5 (*a*) Residual norm *R* and deviation from original force Δ*F* as a function of regularization parameter λ for the data from Fig. 2 *b*, that is distance between micropatterned dots is increased to 4 μm. (*b*) Same for data from Fig. 2 *c*, that is there are 13 focal adhesions with distance 2 μm on each side. (*c*) Same for the case of five focal adhesions with distance 7 μm on each side. The more displacement is picked up and the larger the distance between focal adhesions, the better is the force reconstruction.

We now return to a noise level of $\sigma = 1$ pixel = 0.133 μm, but decrease the density of micropatterned dots, that is, we pick up less displacements. The corresponding displacement data is shown in Fig. 2 *b*: the distance between dots has been doubled from 2 to 4 μm. Fig. 5 *a* shows that now the force reconstruction is even worse than in the case of increased noise: optimal regularization now corresponds to a 45% deviation in reconstructed from original force and goes up to over 70% for the case without regularization. This drastic effect had to be expected, because the relevant information is stored in the displacements that are above the noise level, that is in the displacements close to FAs, of which now many are lost. We also confirmed that the reconstruction is not considerably improved when adding displacements farer away from the cell (data not shown). Note, however, that the procedure of choosing λ is not affected by adding data with little additional information.

In Fig. 5, *b* and *c*, we show the effect of changing the distance between FAs from 4 to 2 μm and 7 μm, respectively (the displacement data for the first case is shown in Fig. 2 *c*). To be able to compare the different case for the same level of noise, $\sigma = 1$ pixel = 0.133 μm, we adjusted the typical force in such a way that the largest displacement picked up remains close to 1.3 μm. This amounts to decreasing and increasing the typical force of 20 nN by ~5 nN, respectively. Then the deviation from original force at optimal regularization, which was 24% in the reference case, goes up to 31% and down to 15% for the two other cases, respectively. Although the corresponding standard deviations for single forces remain in the range of 4 nN, in the first case the spatial resolution is worsened, whereas in the second case it is improved. Moreover, in the case of well-separated focal adhesions, regularization becomes less relevant: in Fig. 5 *c*, there is only little difference in Δ*F* for all values of λ up to λ = 0.04, which is the level of optimal regularization.

In Fig. 6, we show the results of a simple bootstrap analysis for the force reconstruction presented in Fig. 4, that is the same patterns of forces and dots like in Fig. 2 *a*, but

a noise level in the displacement data that is increased to $\sigma = 2$ pixel = 0.266 μm. The average force pattern resulting from this bootstrap analysis is stronger regulated than the initial force estimate, because we did not adjust the regularization parameter λ when doing the bootstrap simulations. However, the bootstrap analysis now allows us to obtain error intervals for the components of the single forces. In the case of optimal regularization with λ = 0.09, Fig. 6 *a*, the error intervals are of more or less constant size around 2 nN. In the case without regularization, Fig. 6 *b*, the error bars are increased to an average size of 6 nN, and are larger if FAs with significant forces are nearby. Note that the error intervals resulting from this kind of bootstrap analysis do not include the original force pattern shown in Fig. 2 *a*, because they reflect only the effect of noise in the displacement data on the force resolution and do not deal with the spatial resolution for which the above analysis showed that it has been lost in this particular case due to the smoothing action of the elastic kernel (compare Fig. 4). In general, more complicated bootstrap procedures could be developed to get more precise estimates of the errors involved.

Micropipette manipulation

As a control experiment, we applied known forces to elastic substrates by lowering a micropipette onto the substrate and then shifting it tangentially. In Fig. 7, we show the numerical analysis of such an experiment in terms of a point-like force applied at the midpoint of the micropipette contact region. The χ-criterion suggests λ = 0.05 (the *L*-curve criterion seems to suggest a somehow smaller value), which leads to a force estimate of *F* = 660 nN. A bootstrap analysis gives an error estimate of 13 nN. From the observed deflection of the micropipette, the applied force can be estimated to be 600 ± 90 nN, so the agreement is good. Note that the force applied by the micropipette is distributed, but because displacements are picked up only in the regions in which the
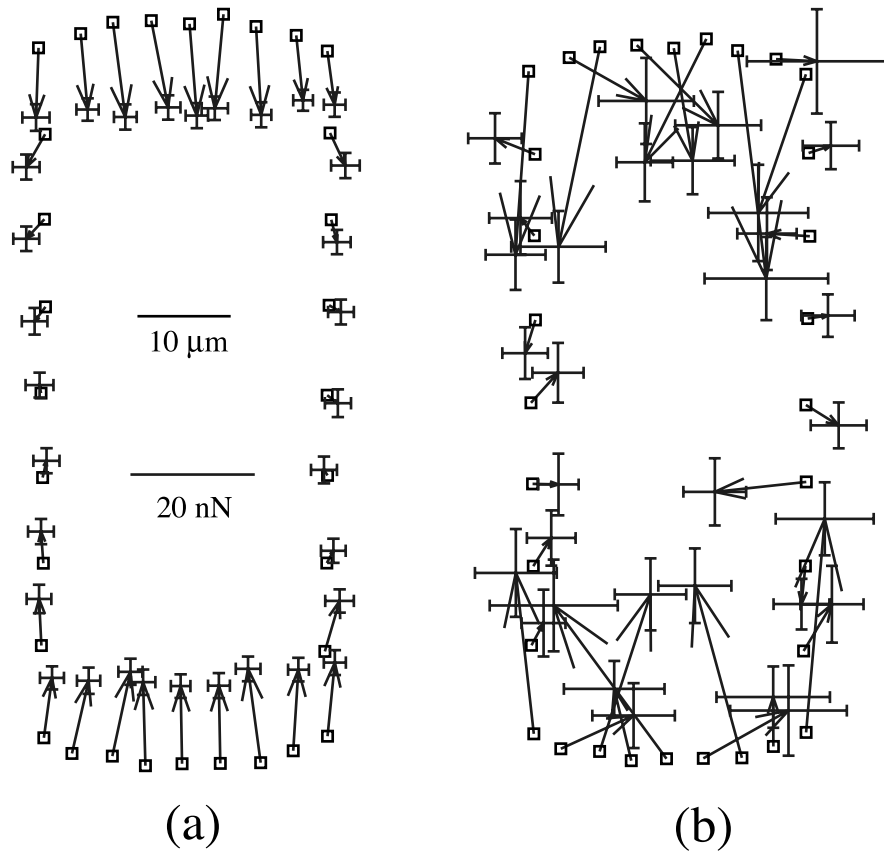
FIGURE 6 Simple bootstrap analysis for the case of Fig. 4, that is for data from Fig. 2 *a*, but with noise level increased to $\sigma = 2$ pixel $= 0.266$ μm. (*a*) Case of optimal regularization, force resolution around 2 nN. (*b*) Case without regularization, force resolution around 6 nN. This kind of bootstrap analysis indicates the effect of noise in the displacement data on the force resolution but does not reflect the spatial resolution.

field of view is not obscured by the micropipette, the force monopole approximation is appropriate. We also analyzed the same displacement data with increasing numbers of point forces distributed over the contact region and confirmed that

this increases the estimate for the overall force only slightly. Moreover, the different forces turn out to be more or less parallel (no twist) and decay if one moves away from the midpoint of the contact region.
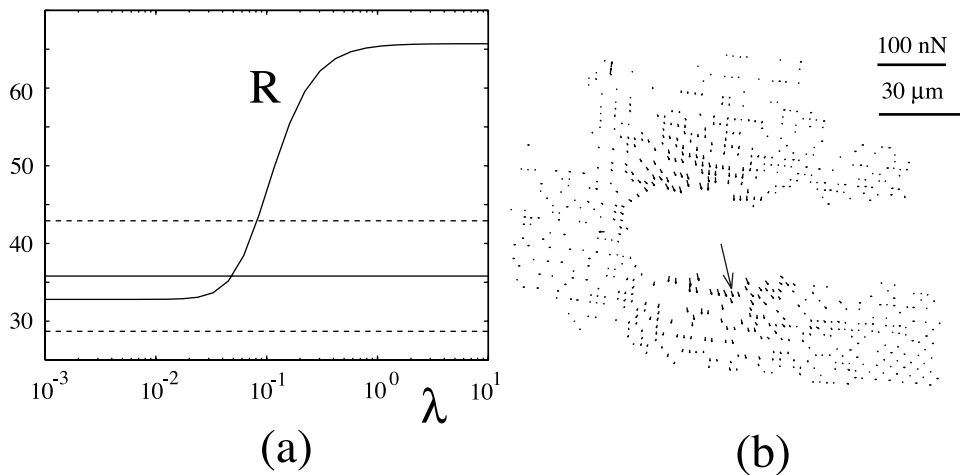

FIGURE 7 Analysis of a micropipette control experiment with one point-like force (Young modulus $E = 12$ kPa). (*a*) Residual norm R as function of regularization parameter λ. (*b*) Force reconstruction according to the χ-criterion ($\lambda = 0.05$). The result $F = 660 \pm 13$ nN for the overall force agrees with the experimental value $F = 600 \pm 90$ nN inferred from the micropipette deflection.
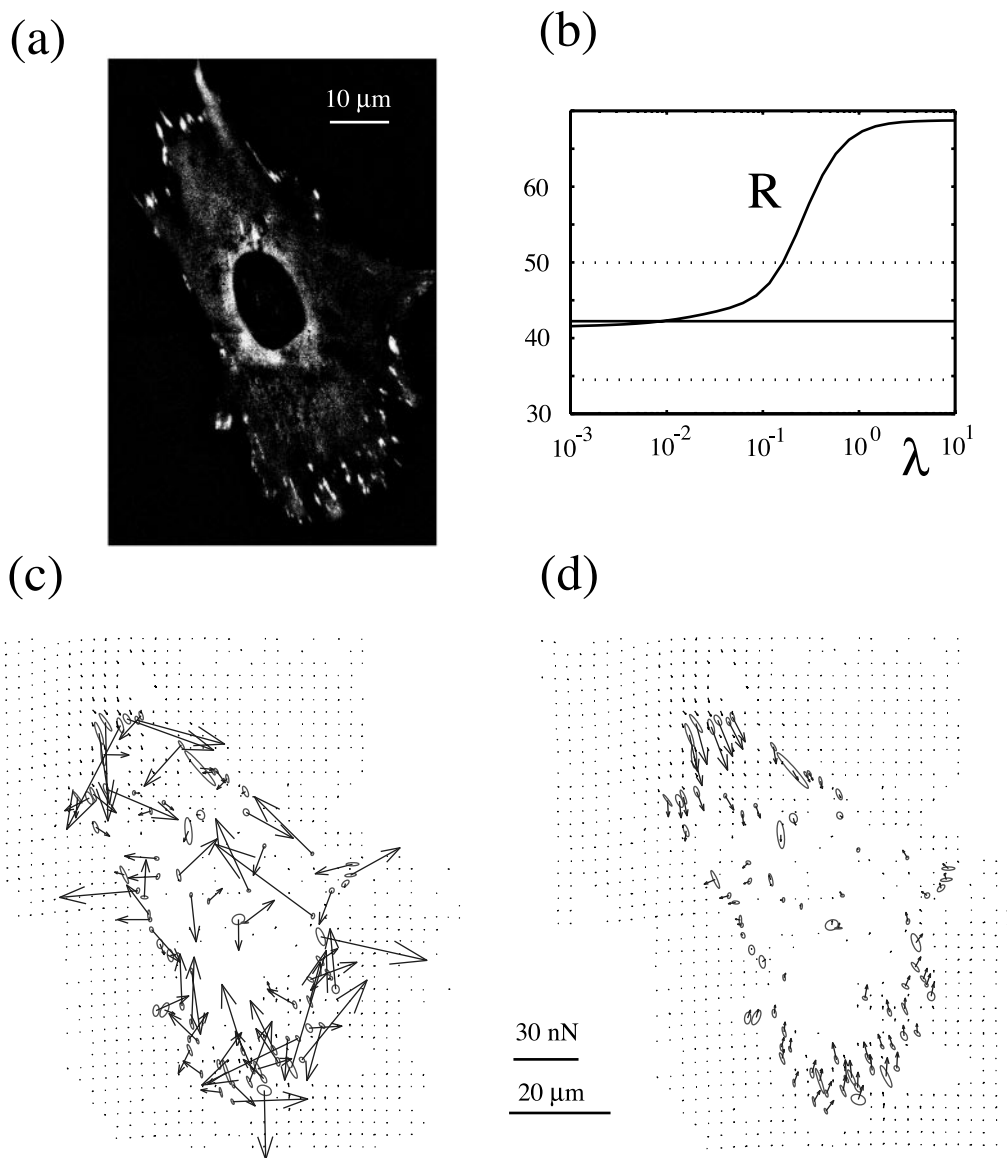
(a)

10 μm

(b)

(c)

(d)

30 nN

20 μm

FIGURE 8   Cell traction from a stationary fibroblast (Young modulus $E = 18$ kPa). (*a*) Fluorescence image of the cell, which is transfected with GFP-vinculin. Vinculin is a major component of focal adhesions and its localization is used to identify the regions, which correspond to large forces. (*b*) Residual norm R as a function of regularization parameter λ for a whole human foreskin fibroblast. (*c*) Force reconstruction for $\lambda = 0.01$ (middle of χ-interval) and (*d*) $\lambda = 0.1$ (upper boundary of χ-interval). In *c*, regularization is too weak, and the force pattern is erratic. In *d*, there is an unexplained drift in the lower part of the force pattern, but the overall force pattern is reasonable. Ellipses are fits to the focal adhesions as marked by GFP vinculin.

Cell traction

The rigidity of our substrates has been optimized for studying traction from strong animal cells like fibroblasts and cardiac myocytes. In Fig. 8, we present the analysis for a whole human foreskin fibroblast. To resolve the displacement, such a high microscope resolution was needed that the cell did not fit into one single picture; the data presented here were assembled from two different pictures taken one after the other. Fig. 8 *a* shows the resulting fluorescence picture for the whole cell, which is strongly polarized. Most FAs are located along the rim of the cell, and more or less elongated along the long axis of the cell itself. The residual norm R as a function of regularization parameter λ is shown in Fig. 8 *b*. We see that the χ-criterion suggests $\lambda = 0.01$. However, the resulting regularization is too weak, as can be seen from the resulting force pattern shown in Fig. 8 *c*, which looks rather erratic. Therefore, we use the upper boundary of the confidence interval, that is $\lambda = 0.1$, which is still consistent with the noise level (this choice also seems to be consistent with the *L*-curve criterion). The resulting force pattern is shown in Fig. 8 *d*. Because we have fitted ellipses to the FAs in Fig. 8, *c* and *d*, one sees clearly that

for the stronger level of regularization, the forces in the upper part of the cell are more or less parallel to the elongation of the single FAs. This seems reasonable because one expects stress fibers to run in the same direction. In the lower part of the cell, the forces seem to be somehow rotated to the right. One reason for this might be that displacement data are rather scarce in this region, so too much information has been lost as to achieve a reliable force reconstruction (the drastic effect of too little displacement information has been shown in Fig. 5 *a*). We find that the force in the upper part can be as strong as 30 nN. In the lower part, most forces are in the order of 10 nN. Note that there are several small FAs at the sides that seem to carry only little force. In general, we find that the cell is highly polarized also in regard to the force pattern and that the two force bearing regions at the upper and lower sides more or less balance each other. Due to Newton's third law, the overall vector force is expected to vanish for a stationary cell, but in this analysis it amounts to 10% of the overall force magnitude, which is probably due to the unreliable force reconstruction in the lower part of the cell. From the viewpoint of a force multipolar expansion, one might say that the cell forms a force contraction dipole of strength $P = -10^{-11}$ J; this corresponds to a pair of forces, separated by a distance of 60 μm and each 200 nN strong. A similar result, $P = -3 \; 10^{-12}$ J, was obtained by Butler and coworkers for a human airway smooth muscle cell (Butler et al., 2002) (there the force dipole tensor is called the moment matrix).

DISCUSSION

In this paper, we presented a novel computational technique that allows to calculate forces at the level of single FAs from displacement data of elastic (micropatterned) substrates and fluorescence data of GFP-vinculin-labeled FAs. Our main assumption is that forces exerted at FAs marked by fluorescent GFP vinculin are appreciably higher than those developed in neighboring regions along the ventral cell membrane. This assumption is based on the fact that we never observed traction near an area deprived of FAs. Our finding that large force corresponds to large FAs seems to justify our assumption a posteriori. Because displacements can be measured only at discrete points, the Fredholm integral equation relating forces to displacements is converted into a system of linear equations. The Boussinesq solution for the Green function of an elastic isotropic half-space is used as kernel for the Fredholm equation. We showed in the framework of a force multipole expansion that the assumption of point-like forces is reasonable as long as displacements are picked up at a distance to the FAs, which is similar to their lateral dimensions. The force multipolar expansion was also used to argue in detail why effects from the clamped boundary conditions at the bottom and at the sides of the polymer film can be neglected in our treatment.

It is well known that Fredholm integral equations of the first kind like the one of linear elasticity theory are ill-posed, irrespective of using the assumptions of localized or distributed force. By extensively simulating artificial data that mimic experimental conditions, we confirmed that in general the inverse elastic problem needs regularization to arrive at a reliable force estimate. In particular we showed that in most realistic cases, the deviation of reconstructed from original force ΔF shows a clear minimum at finite regularization parameter λ. In the absence of this information, that is in real experiments, one has to estimate the optimal value for the regularization parameter λ. We used two different criteria, the χ- (or discrepancy) criterion and the *L*-curve criterion, which lead to identical results for simulated data. For real data, the agreement between the two criteria is less good (possibly due to the presence of non-Gaussian noise or imperfections of the elastic substrate) but still sufficient. In the rare cases that these criteria lead to erratic force patterns (compare Fig. 8 *c*), we used the upper limit of the χ-interval, because it is still consistent with the independently determined noise level.

It is important to note that spatial resolution for the force field is inherently restricted by the smoothing action of the Fredholm integral equation on the length scale $\sqrt{F/E} \approx$ μm, in which $F = 10$ nN is the typical force at FAs and $E = 10$ kPa a typical value for the Young modulus. Our simulations demonstrated that both spatial and force resolutions depend on the details of the displacement and force patterns. Although no generally valid values can be given, simulations for realistic situations showed that our spatial and force resolutions are better than 4 μm and 4 nN, respectively. This values have been derived above for a simulated reference pattern, which is somehow more difficult to reconstruct than experimental force patterns in which the high density of FAs of the reference pattern is realized only at certain regions of the cell. We conclude that calculated forces can be reliably attributed to single FAs if no other FAs are closer than a few micrometers. Simple bootstrap analysis like the one presented in Fig. 6 leads to an estimate for force resolution of 2 nN, but at the same time to a decrease in spatial resolution (which however is not quantified in this scheme). Although the smoothing action of the elastic kernel indicates a basic limitation of elastic substrate experiments, it is worth noting that it also benefits our quantitative analysis, because it allows to neglect corrections arising from the modulation of the micropattern.

The method presented here can now be used to analyse mechanically active cells in quantitative detail. Experimentally, it requires the use of (microstructured) elastic substrates and labeling of the force-transmitting system. We used GFP-vinculin to label FAs, but other possibilities include use of GFP-cDNA-constructs encoding other adhesion-associated proteins (like paxillin, zyxin, alpha-actinin, or actin) or specific antibodies. Numerically, it requires image analysis of the phase contrast and fluorescence pic-

tures and use of the force reconstruction program. As the procedure described here is rather simple and robust, we expect that our protocol might become a standard tool for such a purpose. In contrast to the reconstruction of a continuous stress field (Dembo and Wang, 1999; Lo et al., 2000; Beningo et al., 2001), the reconstruction of a discrete force pattern is computationally rather cheap and needs only minutes on a standard PC. Therefore, it could be used to study mechanical activity of cells in real time. Note that if the force-transmitting system cannot be marked, the standard assumption of distributed force has to be used.

One main result of our analysis of simulated data is the confirmation that in general regularization cannot be neglected when reconstructing force patterns from elastic substrate data. The need for regularization was also demonstrated by real traction data presented in Fig. 8, where insufficient regularization leads to an erratic force pattern. This finding stands in marked contrast to recent work by Butler and coworkers, who suggested a new method that does not involve regularization (Butler et al., 2002). The starting point for this method is the observation that the Fredholm integral equation from Eq. 1 can be easily inverted in Fourier space due to the convolution theorem. Because the experimental data at hand is not spatially periodic, the back transform introduces artifactual forces at the boundaries of the sample, which the authors claim can be easily distinguished from the cellular forces. Butler and coworkers report that no significant effect of noise can be detected in the reconstructed force pattern. However, this claim is not backed by any detailed analysis of the noise level in the experimental data or of simulated data mimicking the experimental force patterns. In our analysis of simulated data, the necessity for regularization is evidenced by minima in ΔF, the deviation between original and reconstructed force, at finite values of the regularization parameter λ. Examples for this behavior are shown in Fig. 3 *a* for the reference case mimicking our experiments, in Fig. 4 *a* for larger noise level, in Fig. 5 *a* for reduced displacement density, and in Fig. 5 *b* for increased density of FAs. Although it can happen that regularization becomes irrelevant in special cases (like in the case of a decreased density of FAs shown in Fig. 5 *c*), this situation is not generic and should be proven to exist when neglecting regularization of elastic substrate data.

It is interesting to consider which values for the rigidity should be chosen for an elastic substrate experiment. On the one hand, one expects that cells exert exactly the kind of forces that deform other cells. The effective Young modulus of a cell has been measured in AFM-experiments to be of the order of kPa (Radmacher et al., 1996). PDMS-substrates as used in our study have somehow higher rigidities, but smaller rigidities can be achieved with other protocols or materials. On the other hand, there are at least two reasons why the elastic substrate should not be too soft. First, in this case one would expect the force-generating cell to react in

a specific way; in fact it has been observed that an elastic substrate, which is very soft induces the cell to react by weakening the adhesion (Pelham and Wang, 1997). A systematic study of cell adhesion on substrates with varying elastic rigidity has shown that for fibroblasts there exists an optimal elastic substrate rigidity in the kPa range where the cells are maximally elongated (Janmey et al., 2001). Second, we explained above that the spatial resolution in such an experiment is limited to the length scale $\sqrt{F/E}$ due to the smoothing action of the elastic kernel. Thus, decreasing rigidity E leads to decreasing spatial resolution. Therefore, elastic substrates with Young modulus of the order of kPa seem to be the right choice for the task at hand.

Using the method described here, we found that for stationary cells, force and lateral size of FAs show a linear relationship (Balaban et al., 2001). Very recently, it was found that for locomoting fibroblasts, this relationship may be inverse (Beningo et al., 2001). Although that work is also based on quantitative analysis of elastic substrate data, it is important to note that the two studies differ in several aspects. First, it is well known that the organization of the force generating actin system is very different in the two cases (Smilenov et al., 1999). For locomoting cells, numerous small and dot-like FAs constantly form close to the lamellipodium. These so-called focal complexes provide adhesion at the leading edge and are regulated by Rac-signaling (Kraynov et al., 2000). They do not connect to stress fibers but rather provide the substrate anchorage for the expanding actin network in the lamellipodium. Focal complexes can be regarded as precursors for the larger and often streak-like FAs dominating adhesion of stationary cells, which are regulated by Rho-signaling and usually connect to stress fibers. The linear relationship found in our study for stationary cells seems to indicate that in this case, focal contacts grow in a very regular way. In fact, one can speculate that integrins, the cytoplasmic proteins connected to them, and the stress fibers build up a supramolecular complex, which is highly ordered in the lateral dimensions, and that the order of this structure is increased by the force applied to the complex. Recently, it has been shown that FAs in stationary cells act as mechanosensors, which activate the Rho-pathway in response to applied force (Riveline et al., 2001). It is likely that the mechanosensory function is related to conformational or structural changes inside the FA complex. In contrast to stationary cells, for locomoting cells, force is much more isotropically distributed in the rapidly expanding actin network of the lamellipodium. Here it can be speculated that focal complexes are foremost needed to keep the advancing edge close to the substrate and to promote active polymerization. An inverse relationship between force and size might indicate that new complexes are foremost formed close to the regions of large actin activity, which is also the region of largest force. Because in the case of locomoting cells, the force generating system is much

less coupled to the existence of cell-matrix adhesions than for stationary cells, the assumption of most force being localized at well-developed adhesion plaques is not valid in this case, and the force reconstruction has to assume distributed force (Dembo and Wang, 1999; Lo et al., 2000; Beningo et al., 2001).

Second, we want to point out that the data analysis differs in the two studies both with regard to the structural and force properties of the FAs. In the work on locomoting cells, structural strength of a FA was estimated by identifying the pixel of highest fluorescence intensity from GFP-zyxin, and mechanical force was identified with the corresponding value of the continuous stress field reconstructed from the displacement data. In contrast, we found that fluorescence intensity from GFP-vinculin per pixel is constant across a mature FA, and its structural strength was identified with the surface area of an ellipse fitted to its lateral extension as marked by the GFP-vinculin. This quantity we then correlated with the overall force attributed to the FA in the framework of a force multipolar expansion. Thus, the correlation analysis in the two studies is quite different.

Third, it should be noted that we used PDMS-substrates coated with fibronectin, whereas the other group used PAA-substrates coated with type-I collagen. It has been shown that FAs (or parts of it) can translocate over the substrate when pulled upon by cellular forces (Smilenov et al., 1999; Zamir et al., 2000), and in general it has been argued that ECM proteins play an active role in the regulation of cell adhesion (Shaub, 1999; Janmey et al., 2001). Thus, it is likely that the different matrices induce differences in the cellular force patterns.

The main result of our work on cell traction was that there exists a linear relationship between force and area of a FA with an offset for area for vanishing force. This seems to indicate that the development of FAs is divided into two stages. In the initial stage, hardly no force is generated, and it can be speculated that this relates to the fact that integrin signaling suppresses Rho-signaling (Ren et al., 1999). The later stage might be stimulated by Rho-signaling and corresponds to regular growth of a rather compact supramolecular arrangement. This picture naturally explains the linear relationship, because now the addition of new components to the FAs adds a proportional amount of force. Note that such a linear relationship cannot exist for locomoting cells, which have to rupture adhesions at the trailing edge.

REFERENCES

Abercrombie, M., and G. A. Dunn. 1975. Adhesions of fibroblasts to substratum during contact inhibition observed by interference reflection microscopy. *Exp. Cell Res.* 92:57–62.

Balaban, N. Q., U. S. Schwarz, D. Riveline, P. Goichberg, G. Tzur, I. Sabanay, D. Mahalu, S. Safran, A. Bershadsky, L. Addadi, and B. Geiger. 2001. Force and focal adhesion assembly: a close relationship studied using elastic micro-patterned substrates. *Nat. Cell Biol.* 3:466–472.

Beningo, K. A., M. Dembo, I. Kaverina, J. V. Small, and Y.-L. Wang. 2001. Nascent focal adhesions are responsible for the generation of strong propulsive forces in migrating fibroblasts. *J. Cell Biol.* 153: 881–887.

Beningo, K. A., and Y.-L. Wang. 2002. Flexible substrata for the detection of cellular traction forces. *Trends Cell Biol.* 12:79–84.

Burridge, K., and M. Chrzanowska-Wodnicka. 1996. Focal adhesions, contractility, and signaling. *Annu. Rev. Cell Dev. Biol.* 12:463–518.

Burton, K., J. H. Park, and D. L. Taylor. 1999. Keratocytes generate traction forces in two phases. *Mol. Biol. Cell.* 10:3745–3769.

Burton, K., and D. L. Taylor. 1997. Traction forces of cytokinesis measured with optically modified elastic substrata. *Nature.* 385:450–454.

Butler, J. P., I. M. Tolic-Norrelykke, B. Fabry, and J. J. Fredberg. 2002. Traction fields, moments, and strain energy that cells exert on their surroundings. *Am. J. Physiol. Cell Physiol.* 282:C595–C605.

Chen, W., and S. J. Singer. 1982. Immunoelectron microscopic studies of the sites of cell-substratum and cell-cell contacts in cultured fibroblasts. *J. Cell Biol.* 95:205–222.

Chicurel, M. E., C. S. Chen, and D. E. Ingber. 1998. Cellular control lies in the balance of forces. *Curr. Opin. Cell. Biol.* 10:232–239.

Choquet, D., D. F. Felsenfeld, and M. P. Sheetz. 1997. Extracellular matrix rigidity causes strengthening of integrin-cytoskeleton linkages. *Cell.* 88:39–48.

Cukierman, E., R. Pankov, D. R. Stevens, and K. M. Yamada. 2002. Taking cell-matrix adhesions to the third dimension. *Science.* 294: 1708–1712.

Dembo, M., T. Oliver, A. Ishihara, and K. Jacobson. 1996. Imaging the traction stresses exerted by locomoting cells with the elastic substratum method. *Biophys. J.* 70:2008–2022.

Dembo, M., and Y.-L. Wang. 1999. Stresses at the cell-to-substrate interface during locomotion of fibroblasts. *Biophys. J.* 76:2307–2316.

Efron, B., and R. J. Tibshirani. 1993. An introduction to the bootstrap. *in* Monographs on Statistics and Applied Probability, Vol. 57. Chapman and Hall, New York.

Finer, J. T., R. M. Simmons, and J. A. Spudich. 1994. Single myosin molecule mechanics: piconewton forces and nanometer steps. *Nature.* 368:113–119.

Galbraith, C. G., and M. P. Sheetz. 1997. A micromachined device provides a new bend on fibroblast traction forces. *Proc. Natl. Acad. Sci. U.S.A.* 94:9114–9118.

Galbraith, C. G., and M. Sheetz. 1998. Forces on adhesive contacts affect cell function. *Curr. Opin. Cell Biol.* 10:566–571.

Geiger, B., and A. Bershadsky. 2001. Assembly and mechanosensory function of focal contacts. *Curr. Opin. Cell Biol.* 13:584–592.

Geiger, B., A. Bershadsky, R. Pankov, and K. M. Yamada. 2001. Transmembrane crosstalk between the extracellular matrix and the cytoskeleton. *Nat. Rev. Mol. Cell Biol.* 2:793–805.

Hansen, P. C. 1998. Rank-deficient and discrete ill-posed problems. *in* SIAM monographs on mathematical modeling and computation. SIAM, Philadelphia, PA.

Harris, A. K., D. Stopak, and P. Wild. 1981. Fibroblast traction as a mechanism for collagen morphogenesis. *Nature.* 290:249–251.

Harris, A. K., P. Wild, and D. Stopak. 1980. Silicone rubber substrata: a new wrinkle in the study of cell locomotion. *Science.* 208:177–179.

Honerkamp, J., and J. Weese. 1990. Tikhonovs regularization method for ill-posed problems. *Continuum Mech. Thermodyn.* 2:17–30.

Janmey, P. A., T. Yeung, and L. A. Flanagan. 2001. Effect of substrate stiffness on cell morphology. *Abstracts ASME Summer Bioeng. Conf.* 50:709–710.

Kraynov, V. S., C. Chamberlain, G. M. Bokoch, M. A. Schwartz, S. Slabaugh, and K. M. Hahn. 2000. Localized Rac activation dynamics visualized in living cells. *Science.* 290:333–337.

Landau, L. D., and E. M. Lifshitz. 1970. Theory of elasticity. 2nd Ed. Course of Theoretical Physics, Vol. 7. Pergamon Press, Oxford.

Lee, J., M. Leonard, T. Oliver, A. Ishihara, and K. Jacobson. 1994. Traction forces generated by locomoting keratocytes. *J. Cell Biol.* 127: 1957–1964.

Lo, C.-M., H.-B. Wang, M. Dembo, and Y.-L. Wang. 2000. Cell movement is guided by the rigidity of the substrate. *Biophys. J.* 79:144–152.

Merkel, R., P. Nassoy, A. Leung, K. Ritchie, and E. Evans. 1999. Energy landscapes of receptor-ligand bonds explored with dynamic force spectroscopy. *Nature.* 397:50–53.

Oliver, T., M. Dembo, and K. Jacobson. 1999. Separation of propulsive and adhesive traction stresses in locomoting keratocytes. *J. Cell Biol.* 145:589–604.

Pelham, R. J., and Y.-L. Wang. 1997. Cell locomotion and focal adhesions are regulated by substrate flexibility. *Proc. Natl. Acad. Sci. U.S.A.* 94:13661–13665.

Press, W. H., S. A. Teukolsky, W. T. Vetterling, and B. P. Flannery. 1992. Numerical recipes in FORTRAN. The art of scientific computing. 2nd Ed. Cambridge University Press, Cambridge.

Radmacher, M., M. Fritz, C. M. Kacher, J. P. Cleveland, and P. K. Hansma. 1996. Measuring the viscoelastic properties of human platelets with the Atomic Force Microscope. *Biophys. J.* 70:556–567.

Ren, X. D., W. B. Kiosses, and M. A. Schwartz. 1999. Regulation of the small GRP-binding protein Rho by cell adhesion and the cytoskeleton. *EMBO J.* 18:578–585.

Rief, M., M. Gautel, F. Oesterhelt, J. M. Fernandez, and H. E. Gaub. 1997. Reversible unfolding of individual titin immunoglobulin domains by AFM. *Science.* 276:1109–1112.

Riveline, D., E. Zamir, N. Q. Balaban, U. S. Schwarz, B. Geiger, Z. Kam, and A. D. Bershadsky. 2001. Focal contact as a mechanosensor: externally applied local mechanical force induces growth of focal contacts by a mDial-dependent and ROCK-independent mechanism. *J. Cell Biol.* 153:1175–1185.

Shaub, A. 1999. Unravelling the extracellular matrix. *Nat. Cell Biol.* 1:E173–E175.

Smilenov, L., A. Mikhailov, R. J. Pelham, E. E. Marcantonio, and G. G. Gundersen. 1999. Focal adhesion motility revealed in stationary fibroblasts. *Science.* 286:1172–1174.

Thoumine, O., A. Ott, and D. Louvard. 1996. Critical centrifugal forces induce adhesion rupture or structural reorganization in cultured cells. *Cell Motil. Cytoskeleton.* 33:276–287.

Zamir, E., B.-Z. Katz, S. Aota, K. M. Yamada, B. Geiger, and Z. Kam. 1999. Molecular diversity of cell-matrix adhesions. *J. Cell Sci.* 112: 1655–1669.

Zamir, E., M. Katz, Y. Posen, N. Erez, K. M. Yamada, B. Z. Katz, S. Lin, D. C. Lin, A. Bershadsky, Z. Kam, and B. Geiger. 2000. Dynamics and segregation of cell-matrix adhesions in cultured fibroblasts. *Nat. Cell Biol.* 2:191–196.